

Electron energy loss spectroscopy of wall charges in plasma-facing dielectrics

E. Thiessen, F. X. Bronold, and H. Fehske

Institut für Physik, Universität Greifswald, 17489 Greifswald, Germany

(Dated: July 30, 2021)

We propose a setup enabling electron energy loss spectroscopy to determine the density of the electrons accumulated by an electro-positive dielectric in contact with a plasma. It is based on a two-layer structure inserted into a recess of the wall. Consisting of a plasma-facing film made out of the dielectric of interest and a substrate layer the structure is designed to confine the plasma-induced surplus electrons to the region of the film. The charge fluctuations they give rise to can then be read out from the backside of the substrate by near specular electron reflection. To obtain in this scattering geometry a strong charge-sensitive reflection maximum due to the surplus electrons the film has to be most probably pre-n-doped and sufficiently thin with the mechanical stability maintained by the substrate. We demonstrate the feasibility of the proposal by calculating the loss spectrum for an Al_2O_3 film on top of a CaO layer. We find a reflection maximum strongly shifting with the density of the surplus electrons and suggest to use it for its diagnostics.

PACS numbers: 79.20.Uv, 73.30.+y, 52.40.Kh

I. INTRODUCTION

The most fundamental manifestation of the interaction of a plasma with a solid is the formation of an electric double layer consisting, respectively, of an electron-depleted and electron-rich space charge region on the plasma and the solid side of the interface¹. It arises because electrons are deposited more efficiently onto or into the surface, depending on its electronic structure, than they are extracted from it by neutralization/de-excitation of ions/radicals². Since the beginning of gaseous electronics³ it is of course known that an electric double layer is formed at plasma-solid interfaces. Yet a microscopic understanding of the solid-based part of the double layer is still missing, mostly because of the limitations of the diagnostics for surface charges and because it was so far—perhaps—not essential for the success of plasma physics and technology. Continuing progress in the miniaturization of integrated microdischarges^{4,5}, however, driven by the desire to combine solid-state and gaseous electronics^{6,7}, makes the embracing solid structure an integral part of the plasma-device. In these structures the solid- and plasma-based charge dynamics are intimately linked. A complete understanding of the discharge requires thus to upgrade plasma diagnostics by techniques which provide also a view on the charge dynamics inside the plasma-facing solid.

There exist a number of techniques to estimate the charge accumulated by plasma-facing solids. Electric probes⁸, surface potential measurements^{9–11}, optomechanical devices based on the reflection of a laser by a cantilever¹², and the Pockels effect of an electro-optic crystal^{13–18} have been employed for that purpose. However, with the exception of the Pockels effect measurements, the methods are rather invasive. In addition, they are limited to measuring the total charge accumulated by the plasma-facing solid. How the charge is distributed normal to the plasma-wall interface cannot be determined. Information about the charge dynamics in-

side the solid can also not be obtained by these methods.

To overcome the limitations of the existing methods we recently proposed infrared attenuated reflection (IR-ATR) spectroscopy as a tool for gaining access to the surplus charges in a dielectric exposed to a plasma¹⁹. The proposal relies on a layered structure supporting a Berreman mode in the infrared which turns out to be rather charge-sensitive. Combined with a self-consistent description of the electric double layer at the plasma-solid interface the method has the potential to provide not only the total charge deposited into the solid (which we demonstrated by an exploratory calculation¹⁹) but also its spatial distribution inside the solid.

Another experimental technique of solid state physics—electron energy loss spectroscopy (EELS) (see Refs.^{20–25} for a general introduction)—could be perhaps also used as a diagnostics for the electrons accumulated by a plasma-facing solid. EELS is an electron reflection technique where the probing electron couples to the dipole fields of the charge fluctuations inside the solid. As a result it loses energy as well as momentum and scatters a bit off the specular direction. The cross section for the near specular reflection contains thus information about charge fluctuations inside the solid.

In a number of experiments it was shown that EELS

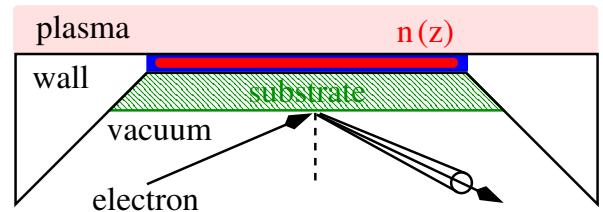


Figure 1: Illustration of the proposed setup for measuring the plasma-induced wall charge by electron energy loss spectroscopy. The idea is to confine the wall charge $n(z)$ in a thin film, stabilize it by a substrate, and read out the charge information with an electron beam applied from the backside.

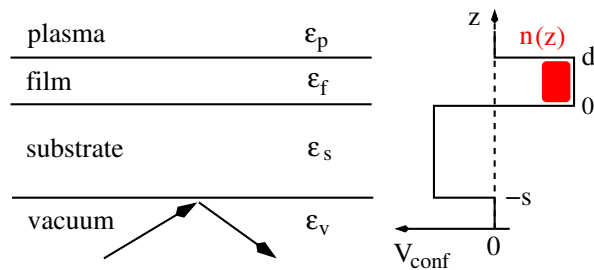


Figure 2: Geometry of the structure we investigate. It consists of an electro-positive film with thickness d and an electro-negative substrate with thickness s embedded between a plasma and a vacuum. The layers as well as the plasma and the vacuum are characterized by background dielectric functions ε_i with $i = p, f, s, v$ as indicated and the electron beam is applied from the vacuum side. On the right is plotted the potential profile confining electrons to the region of the film. It arises from the positive and negative electron affinities χ of the film and the substrate, respectively, and is essential for the operation of the charge measuring device we propose.

can be used to determine parameters characterizing the inhomogeneous electron gases formed at semiconductor surfaces^{26–30}. If it were not for the fact that the plasma prevents applying the probing electron beam directly to the plasma-solid interface it would be clear that EELS can be used as a wall charge diagnostics in plasma applications. To enable EELS to measure the charge accumulated by a plasma-facing solid an indirect setup has to be used. It is the purpose of this paper to describe such a setup and to demonstrate by a model calculation its feasibility as a testbed for investigating the charging of solids exposed to a plasma.

As a first step we focus on a setup measuring the total charge accumulated by an electro-positive dielectric in contact with a plasma, leaving modifications required for an analysis of the depth profile for future work. The setup is shown in Fig. 1. It consists of a film made out of the dielectric of interest in contact with the plasma and supported by a substrate layer. The electron beam supposed to read out the charge information is applied from the side opposite to the plasma-solid interface. Interference with the plasma is thus excluded on the expense of using a thin film structure. For the setup to work it has to be designed in a particular manner. Our calculations indicate the probing electron beam to be sensitive to the fluctuations of the plasma-induced surplus electrons in the film if the thickness of the whole structure is in the sub-100 nm range. In addition we found it advantageous to confine the surplus electrons coming from the plasma to the region of the film by the line-up of the conduction band edges of the film and the substrate. To compensate for the loss of signal strength due to the substrate we suggest moreover to pre-n-dope the plasma-facing film. The last measure is not of principal importance. It is only required for making the signal detectable with EELS instrumentation currently available.

The outline of the rest of the paper is as follows. In

the next section we calculate the cross section for near specular electron reflection from a two-layer structure in contact with a plasma. Due to the confinement of the charge to a thin film the de Broglie wavelength of the electrons is on the same order as the screening length forcing us to employ the nonlocal response theory of Mills and coworkers^{31–33}. Numerical results for an Al_2O_3 film on top of a CaO layer, which is a material combination meeting the requirements listed above, are then presented in Section III. For film thicknesses on the order of a few 10s nanometers and background dopings on the order of 10^{18} cm^{-3} we find a maximum in the reflection cross section due to the collective excitation of the total number of electrons in the film which is sufficiently strong to be detectable and charge-sensitive to serve as a diagnostics for the density of the film's surplus electrons coming from the plasma. Section IV concludes the presentation by summarizing its main points.

II. THEORETICAL BACKGROUND

We consider EELS in an unusual geometry where the probing electron approaches a layered structure of finite width from the side opposite to the interface of interest, which—in our case—is the interface between a plasma and an upper most layer of a stack of materials. As illustrated in Fig. 2, the structure and its embedding are characterized by a set of dielectric functions ε_i with $i = v, s, f, p$ and a potential profile $V_{\text{conf}}(z)$ accounting for the offsets of the layer's conduction band edges from the potential just outside the structure (electron affinities χ). The energy loss we want to detect and use as a charge diagnostics arises from the density $n(z)$ of electrons accumulated in the film next to the plasma. For simplicity we characterize the plasma by a dielectric function ε_p which we moreover set at the end to ε_v neglecting thereby charge fluctuations inside the plasma. To take them into account is beyond the scope of the present work. It constitutes however no principal problem.

A. Cross section for EELS

Using the coordinate system of Fig. 2 and assuming charge fluctuations to arise solely from the stack of materials the microscopic approach developed by Mills³¹ gives for the momentum-integrated EELS cross section

$$\frac{dS}{d\omega} = \frac{2e^2}{\pi\hbar} |R_I|^2 \int_D d^2q_{\parallel} R(\vec{q}_{\parallel}, \omega) P(\vec{q}_{\parallel}, \omega) \quad (1)$$

with $|R_I|^2$ the probability for quantum-mechanical reflection from the vacuum-substrate interface, which we set in the following to unity, the surface-rider function

$$R(\vec{q}_{\parallel}, \omega) = \frac{v_{\perp}^2}{[v_{\perp}^2 q_{\parallel}^2 + (\omega - \vec{v}_{\parallel} \cdot \vec{q}_{\parallel})^2]^2}, \quad (2)$$

accounting for the scattering kinematics, where \vec{v}_{\parallel} and \vec{v}_{\perp} are the electron's velocity components parallel and

perpendicular to the surface, and the loss function ($a = |\vec{a}|$ for any vector \vec{a})

$$P(\vec{q}_{\parallel}, \omega) = \frac{e^2}{\hbar} \int d^2 x_{\parallel} \int_{-\infty}^{\infty} dt e^{i\vec{q}_{\parallel} \cdot \vec{x}_{\parallel} - i\omega t} \int_{-s}^d dz \int_{-s}^d dz' e^{-q_{\parallel}(z+z'+2s)} \langle \delta\rho^{\dagger}(\vec{x}_{\parallel}, z'; t) \delta\rho(0, z; 0) \rangle_T, \quad (3)$$

taking the transfer of energy $\hbar\omega$ and lateral momentum \vec{q}_{\parallel} parallel to the xy -plane from the electron to the solid structure into account. It forces the out-going branch of the scattering trajectory to deviate a bit from the specular direction and carries therefore the information we are looking for.

To the EELS signal not all lateral momenta \vec{q}_{\parallel} contribute to the cross section. Switching to cylindrical coordinates with the polar angle ϕ measured with respect to \vec{v}_{\parallel} one realizes that the integration domain D relevant for EELS is bounded by the ellipse equation²¹,

$$\frac{1}{[q_{\parallel}^c(\phi)]^2} = \frac{\sin^2(\phi)}{[q_{\parallel}^{\max}]^2} + \frac{\cos^2(\phi)}{[q_{\parallel}^{\max} \cos(\phi_i)]^2}, \quad (4)$$

where ϕ_i is the incident angle of the probing beam with respect to the surface normal, $q_{\parallel}^{\max} = q_{\text{dB}}\phi_a$, with $q_{\text{dB}} = \sqrt{2E_0 m}/\hbar$ the de Broglie wave number of the scattering electron incoming with energy E_0 and ϕ_a half of the acceptance angle of the detector.

The essential part of the cross section is the loss function $P(\vec{q}_{\parallel}, \omega)$ which via (3) is related to the charge-charge correlation function $\langle \delta\rho^{\dagger}(\vec{x}_{\parallel}, z', t) \delta\rho(0, z, 0) \rangle_T$, where the operator $\delta\rho(\vec{x}_{\parallel}, z', t)$ describes the charge fluctuations arising in the spatial region for which $-s < z < d$ and the brackets denote the thermodynamical average taken over this domain at temperature T . Clearly this is an approximation. It assumes that the plasma-facing structure is in thermal equilibrium. In reality this is not the case. But at this early stage of exploring EELS as a charge diagnostics the equilibrium assumption seems justified. Including the non-equilibrium aspects would unnecessarily mask the basic idea we want to convey and will be subject of future work.

From the integrand in (3) arises a problem for the from-the-back detection of the EELS signal. Because of the substrate layer the absolute value of the argument of the exponential function is even in the most favorite situation $q_{\parallel}s$ with s the thickness of the substrate and²⁸

$$q_{\parallel} \simeq \sqrt{\frac{2m_e}{\hbar^2}} \frac{\hbar\omega \sin \phi_i}{2\sqrt{E_0}} \quad (5)$$

the momentum transferred from the electron to the solid; $\hbar\omega$ is the energy of the charge fluctuation to be detected and m_e is the electron mass. Compared to a system without substrate the EELS signal is hence suppressed by a

factor $\exp(-q_{\parallel}s)$ implying for $s \simeq q_{\parallel}^{-1}$ the intensity to be down by roughly 37%. Thin substrates are thus required for strong signals but they have to be also mechanically stable limiting in practice how thin they can be.

B. Charge fluctuations

We are interested in the EELS fingerprint of the electrons residing in the plasma-facing film. To identify their contribution to (1) we have to isolate the film's electronic charge fluctuation $\delta\rho_e$ from the total charge fluctuation $\delta\rho$ of the two-layer structure. An elegant scheme to accomplish this, due originally to Ehlers and Mills³², who used it to describe EELS from space charge regions at semiconductor surfaces, is based on a consideration of the potential fluctuations outside the solid probed by the EELS electron; subsequently Streight and Mills³³ applied it also to EELS from semiconducting films. Adopted to our situation the potential fluctuations in the region $z < -s$ arising from the charge fluctuations in the region $z > -s$ have to be calculated. On the one hand, this can be done by using the general expression for the electric potential and expanding the factor $|\vec{x} - \vec{x}'|^{-1}$ in terms of surface waves²⁰. It can be however also obtained by solving for a point charge located in the film the Poisson equation with boundary conditions appropriate for the two-layer structure under consideration. Weighting the result with the distribution $\delta\rho_e(\vec{q}_{\parallel}, z, t)$ of surplus electrons in the film gives then an alternative expression for the potential fluctuations which via comparison with the former allows to relate $\delta\rho_e(\vec{q}_{\parallel}, z, t)$ to $\delta\rho(\vec{q}_{\parallel}, z, t)$.

The first approach, based on the general expression for the electric potential in front of the stack, leads to

$$\delta\Phi(\vec{x}, t) = \int \frac{d^2 q_{\parallel}}{(2\pi)^2} e^{i\vec{q}_{\parallel} \cdot \vec{x}_{\parallel}} \delta\Phi(\vec{q}_{\parallel}, z, t) \quad (6)$$

with $z < -s$ and

$$\delta\Phi(\vec{q}_{\parallel}, z, t) = \frac{2\pi e}{q_{\parallel}} \int_{-s}^d dz' e^{q_{\parallel}(z-z')} \delta\rho(\vec{q}_{\parallel}, z', t). \quad (7)$$

The imbedding strategy, on the other hand, working with the Poisson equation,

$$\nabla \cdot [\varepsilon(z) \nabla \Phi(\vec{x})] = -4\pi e \delta(x') \delta(y') \delta(z' - z), \quad (8)$$

where the point charge is located at $x' = y' = 0$ and $d > z' > 0$, that is, inside the film, yields upon utilizing the homogeneity in the xy -plane,

$$\Phi(\vec{x}) = \int \frac{d^2 q_{\parallel}}{(2\pi)^2} e^{i\vec{q}_{\parallel} \cdot \vec{x}_{\parallel}} \Phi(q_{\parallel}, z) \quad (9)$$

with

$$\Phi(q_{\parallel}, z) = A e^{q_{\parallel} z} + B e^{-q_{\parallel} z} \quad (10)$$

and expansion coefficients A and B determined from the boundary conditions appropriate for the z -dependent dielectric function

$$\varepsilon(z) = \begin{cases} \varepsilon_v & \text{for } z < -s \\ \varepsilon_s & \text{for } -s < z < 0 \\ \varepsilon_f & \text{for } 0 < z < d \\ \varepsilon_p & \text{for } z > d \end{cases} . \quad (11)$$

For the imbedding strategy to be applicable the imaginary parts of the dielectric functions ε_i have to be of course negligible in the frequency range of interest. Enforcing the boundary conditions

$$\Phi(q_{\parallel}, z^-) = \Phi(q_{\parallel}, z^+) \quad (12)$$

$$\varepsilon(z^-) \frac{d\Phi(q_{\parallel}, z)}{dz} \Big|_{z^-} - \varepsilon(z^+) \frac{d\Phi(q_{\parallel}, z)}{dz} \Big|_{z^+} = \begin{cases} 4\pi e & \text{if } z = z' \\ 0 & \text{else} \end{cases} \quad (13)$$

at $z = -s$, $z = 0$, and $z = d$ and setting $B = 0$ for $z < -s$ and $A = 0$ for $z > d$ we find—after weighting the result with the (instantaneous) charge distribution inside the film and Fourier transforming the lateral spatial variables—for the potential in the region $z < -s$, denoted now again by $\delta\Phi(\vec{q}_{\parallel}, z, t)$, the expression

$$\delta\Phi(\vec{q}_{\parallel}, z, t) = \frac{(2\pi e/q_{\parallel})4\varepsilon_s}{(\varepsilon_f + \varepsilon_s)(\varepsilon_s + \varepsilon_v)h(q_{\parallel}; \varepsilon_s, s; \varepsilon_f, d; \varepsilon_p, \varepsilon_v)} \int_{-s}^d dz' e^{q_{\parallel}(z-z')} F(q_{\parallel}, z'; \varepsilon_f, d; \varepsilon_p) \delta\rho_e(\vec{q}_{\parallel}, z', t) \theta(z') , \quad (14)$$

with the auxiliary functions

$$h(q_{\parallel}; \varepsilon_s, s; \varepsilon_f, d; \varepsilon_p, \varepsilon_v) = 1 + L_{sv} L_{fs} e^{-2q_{\parallel} s} - L_{fp} L_{fs} e^{-2q_{\parallel} d} - L_{fp} L_{sv} e^{-2q_{\parallel} (d+s)} \quad (15)$$

and

$$F(q_{\parallel}, z; \varepsilon_f, d; \varepsilon_p) = 1 + L_{fp} e^{-2q_{\parallel} (d-z)} , \quad (16)$$

where

$$L_{ij} = \frac{\varepsilon_i - \varepsilon_j}{\varepsilon_i + \varepsilon_j} \quad \text{with } i, j = v, s, f, p . \quad (17)$$

Comparison of (7) and (14) yields then a relation between $\delta\rho(\vec{q}_{\parallel}, z', t)$ and $\delta\rho_e(\vec{q}_{\parallel}, z', t)$ which inserted into (3) leads after some algebra to the loss function

$$P(\vec{q}_{\parallel}, \omega) = 2e^2(1 + n(\omega)) \left[\frac{4\varepsilon_s}{(\varepsilon_f + \varepsilon_s)(\varepsilon_s + \varepsilon_v)h(q_{\parallel}; \varepsilon_s, s; \varepsilon_f, d; \varepsilon_p)} \right]^2 \int_0^d dz \int_0^d dz' e^{-q_{\parallel}(z+z'+2s)} F(q_{\parallel}, z; \varepsilon_f, d; \varepsilon_p) F(q_{\parallel}, z'; \varepsilon_f, d; \varepsilon_p) \text{Im}\chi(\vec{q}_{\parallel}, \omega; z, z') \quad (18)$$

with $n(\omega)$ the Bose distribution function with $\beta = 1/(k_B T)$ and

$$\chi(\vec{q}_{\parallel}, \omega; z, z') = \frac{i\theta(\omega)}{\hbar} \langle [\delta\rho_e^\dagger(\vec{q}_{\parallel}, z, \omega), \delta\rho_e(\vec{q}_{\parallel}, z', 0)] \rangle_T \quad (19)$$

the (commutator) density-density response function for the surplus electrons^{32,33}. The calculation of the loss function $P(\vec{q}_{\parallel}, \omega)$ has thus been reduced to the determination of the function $\chi(\vec{q}_{\parallel}, \omega; z, z')$. That the electrons are embedded in a dielectric structure is taken into account in (18) by the functions in front of $\text{Im}\chi(\vec{q}_{\parallel}, \omega; z, z')$.

C. Density-density response function

The simplest scheme for obtaining the density-density response function $\chi(\vec{q}_{\parallel}, \omega; z, z')$ relies on the random-phase approximation. As in the work of Mills and coworkers^{32,33} it is based on the integral equation,

$$\chi(\vec{q}_{\parallel}, \omega; z, z') = \chi_0(\vec{q}_{\parallel}, \omega; z, z') - \int_0^d dz'' K(\vec{q}_{\parallel}, \omega; z, z'') \chi(\vec{q}_{\parallel}, \omega; z'', z') , \quad (20)$$

where the kernel

$$K(\vec{q}_{\parallel}, \omega; z, z') = \int_0^d dz'' \chi_0(\vec{q}_{\parallel}, \omega; z, z'') v(q_{\parallel}; z'', z') \quad (21)$$

includes the electron-electron interaction $v(q_{\parallel}; z, z')$ and the irreducible particle-hole propagator $\chi_0(\vec{q}_{\parallel}, \omega; z, z')$. Writing for the interaction potential $v(q_{\parallel}; z, z') = e\Phi(q_{\parallel}, z, z')$, with $\Phi(q_{\parallel}, z, z')$ the electric potential at z induced by a point charge at z' , where both z and z' are inside the film, the solution of the Poisson equation (8) can be utilized to deduce

$$v(q_{\parallel}; z, z') = \frac{2\pi e^2}{q_{\parallel} \varepsilon_f} \frac{g(q_{\parallel}; \varepsilon_s, s; \varepsilon_f, d; \varepsilon_p, \varepsilon_v)}{h(q_{\parallel}; \varepsilon_s, s; \varepsilon_f, d; \varepsilon_p, \varepsilon_v)} \quad (22)$$

where

$$g(q_{\parallel}; \varepsilon_s, s; \varepsilon_f, d; \varepsilon_p, \varepsilon_v) = e^{-q_{\parallel}|z-z'|} + L_{sv} e^{-q_{\parallel}(z+z'+2s)} + L_{fs} e^{-q_{\parallel}(z+z')} + L_{fp} e^{-q_{\parallel}(2d-(z+z'))} + L_{sv} L_{fs} e^{-q_{\parallel}(2s+|z-z'|)} + L_{sv} L_{fp} e^{-q_{\parallel}(2(s+d)-|z-z'|)} + L_{fs} L_{fp} e^{-q_{\parallel}(2d-|z-z'|)} + L_{sv} L_{fs} L_{fp} e^{-q_{\parallel}(2(d+s)-(z+z'))} . \quad (23)$$

To complete the construction of the kernel (21) we also need the irreducible electron-hole propagator $\chi_0(\vec{q}_{\parallel}, \omega; z, z')$. It is given by^{32,33}

$$\chi_0(\vec{q}_{\parallel}, \omega; z, z') = \frac{2}{A} \sum_{\vec{k}_{\parallel}} \sum_{i,j} \frac{f(\vec{k}_{\parallel}, i) - f(\vec{k}_{\parallel} + \vec{q}_{\parallel}, j)}{\hbar\omega + i\delta + E_{\vec{k}_{\parallel} + \vec{q}_{\parallel}, j} - E_{\vec{k}_{\parallel}, i}} \cdot \psi_i^*(z) \psi_i(z') \psi_j(z) \psi_j^*(z'), \quad (24)$$

where

$$f(\vec{k}_{\parallel}, i) = \frac{1}{e^{\beta(E_{\vec{k}_{\parallel}, i} - \mu)} + 1} \quad (25)$$

is the Fermi distribution function with $\beta = 1/(k_B T)$ and μ is the chemical potential; A is the quantization area in the xy -plane.

The single electron energies entering (24) contain the energy of the lateral and the vertical motion,

$$E_{\vec{k}_{\parallel}, i} = \frac{\hbar^2 k_{\parallel}^2}{2m^*} + \varepsilon_i \quad (26)$$

with the energy ε_i belonging to $\psi_i(z)$, the part of the wave function describing the perpendicular motion. To obtain ε_i and $\psi_i(z)$ we assume the film to constitute an infinitely deep potential well. Both quantities can then be looked up in textbooks about quantum mechanics³⁴. It is thus not necessary to list them here. Since the electron affinity of Al_2O_3 , the material we will take for the film, is large and positive, the infinitely deep quantum well is a reasonable approximation. Improvements are possible but will be not addressed in this paper. The labels i, j are the quantum numbers labeling the eigenstates of the well and δ is a small but finite number preventing numerical instability. For the results discussed in the next section $\delta = 10^{-5}$. Finally, the chemical potential μ has to be determined. It is related to the surface charge density through the condition³⁵

$$n_s = \frac{m^*}{\pi \hbar^2 \beta} \sum_i \ln(1 + e^{-\beta(\varepsilon_i - \mu)}). \quad (27)$$

Inside the film the electrons are distributed according to

$$n(z) = \frac{m^*}{\pi \hbar^2 \beta} \sum_i \ln(1 + e^{-\beta(\varepsilon_i - \mu)}) |\psi_i(z)|^2, \quad (28)$$

which after integration over z yields (27), as it should, because of the normalization of the wave functions.

D. Remarks concerning the numerics

The numerical work consists of two major parts: (i) calculating the density-density response function $\chi(\vec{q}_{\parallel}, \omega; z, z')$ by solving the integral equation (20) and (ii) integrating $\chi(\vec{q}_{\parallel}, \omega; z, z')$ over z and z' as specified in

(18) to obtain the loss function $P(\vec{q}_{\parallel}, \omega)$, which is then inserted into (1) to yield after integrating over \vec{q}_{\parallel} the EELS cross section $dS/d\omega$.

In order to obtain $\chi(\vec{q}_{\parallel}, \omega; z, z')$ we first have to construct the function $\chi_0(\vec{q}_{\parallel}, \omega; z, z')$. For that purpose we closely follow Ehlers and Mills³² and adopt their approach to the layered structure we consider. Hence, we convert the summation over \vec{k}_{\parallel} to an integral and rewrite (24) using Green functions. Only one sum over the eigenstate labels i remains then. Due to the homogeneity in the xy plane it turns out that all quantities depend only on the absolute value of \vec{q}_{\parallel} which is chosen parallel to the x -direction. For the solution of the integral equation (20) itself we no longer follow Ehlers and Mills³². Instead we employ the numerical strategy Streight and Mills³³ used in their study of semiconducting films. They noticed that for a film the numerical work can be greatly reduced by integrating out the variable z' which enters (20) and (18) only as a parameter. Instead of solving (20) for $\chi(q_{\parallel}, \omega; z, z')$, depending as we now known only on q_{\parallel} , we thus solve an integral equation for

$$X(q_{\parallel}, \omega; z) = \int_0^d dz' F(q_{\parallel}, z'; \varepsilon_f, d; \varepsilon_p) e^{-q_{\parallel} z'} \chi(q_{\parallel}, \omega; z, z'), \quad (29)$$

which can be easily derived from (20) and efficiently solved by discretization and matrix inversion.

Obtaining $\chi(q_{\parallel}, \omega; z, z')$ in the manner described is numerically the most challenging task. The integrations specified in (1) and (18), on the other hand, can be performed with standard integration routines. For the numerical work we used dimensionless variables, measuring energies and lengths, respectively, in units of $k_B T$ and $\lambda_* = \sqrt{\hbar^2 / 2m_e^* k_B T}$, where m_e^* is the effective electron mass in the conduction band of the film.

III. RESULTS

We now present results for a setup consisting of a plasma-facing Al_2O_3 film supported by a CaO substrate layer to which an electron beam is applied from below with $E_0 = 5 \text{ eV}$ and $\phi = 45^\circ$. The acceptance angle of the detector is $2\phi_a = 2^\circ$.

The combination of materials meets the criteria we impose for the setup to work as a testbed for measuring the wall charge and also for our theory to be applicable: (i) charge confinement to the film, (ii) dielectric functions with small imaginary parts in the spectral range of interest, and (iii) mechanical stability. Al_2O_3 is an electro-positive dielectric with electron affinity $\chi = 2.58 \text{ eV}$ ³⁹ whereas CaO is electro-negative with $\chi = -0.86 \text{ eV}$ ⁴⁰. Hence, the surplus electrons coming from the plasma will be confined to the film. In the energy range of the charge fluctuation we probe by EELS, the imaginary parts of the dielectric functions are moreover very small. The

	CaO	Al ₂ O ₃
ε_∞	3.3856	3.2
ε_0	—	9.0
$\nu_1[\text{cm}^{-1}]$	300	385
f_1	9	0.3
$\gamma_1[\text{cm}^{-1}]$	32	5.58
$\nu_2[\text{cm}^{-1}]$	—	442
f_2	—	2.7
$\gamma_2[\text{cm}^{-1}]$	—	4.42
$\nu_3[\text{cm}^{-1}]$	—	569
f_3	—	3
$\gamma_3[\text{cm}^{-1}]$	—	11.38
$\nu_4[\text{cm}^{-1}]$	—	635
f_4	—	0.3
$\gamma_4[\text{cm}^{-1}]$	—	12.7

Table I: Parameters entering (30) for the background dielectric functions of CaO³⁶ and Al₂O₃^{37,38}, the materials used, respectively, for the substrate and the film of the proposed EELS setup for measuring the wall charge.

argument enabling us to express the total charge fluctuation as a product of a factor describing the background and a factor describing the surplus electrons is thus justified. Finally, the mechanical properties of the two materials make them suitable for our setup. Their microhardnesses, for instance, are on the same order as the ones for SiO₂ and Si₃N₄ which are used as sub-100 nm membranes in photoelectron microscopy to withstand pressure gaps at vacuum-liquid interfaces⁴¹. We expect therefore the Al₂O₃/CaO system to allow also the construction of film-substrate structures with thicknesses in the sub-100 nm range, as it is required for the EELS signal to be detectable in the setup we consider.

The background dielectric functions for CaO and Al₂O₃ are found in the literature^{36–38}. Fitting experimental data to a set of damped harmonic oscillators they can be written in the form^{36–38}

$$\varepsilon(\omega) = \varepsilon_\infty + \sum_{i=1}^{i=4} \frac{f_i \omega_i^2}{\omega_i^2 - \omega^2 - i\gamma_i \omega} \quad (30)$$

with $\omega_i = 2\pi\nu_i = 2\pi c/\lambda$. The parameters entering this equation are given in Table I for the two materials. Plots of the dielectric functions themselves are shown in Fig. 3, where we also indicate by vertical dashed lines the spectral region where the charge fluctuation occurs whose density dependence we utilize for diagnostic purposes. Clearly, in the relevant spectral range the dielectric functions are essentially real. In addition to the dielectric functions ε and the electron affinities χ we also need the effective electron mass m_e^* in the conduction band of Al₂O₃. In units of the electron mass $m_e^* = 0.4$. The temperature is set to $T = 300$ K in all calculations and $\varepsilon_p = \varepsilon_v = 1$.

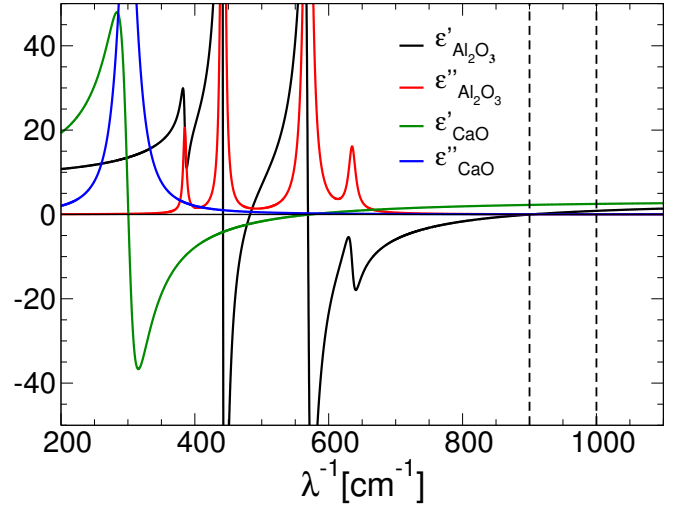


Figure 3: Background dielectric functions for CaO and Al₂O₃ as obtained from (30) using the parameters of Table I. The dashed vertical lines denote the spectral range of the collective excitation of the electrons inside the Al₂O₃ film which we use as a charge diagnostics.

Initially we simulated an undoped stack with thickness 40 nm (which we consider sufficient for mechanical stability) and indeed found a loss peak strongly shifting with the density of the surplus electrons accumulated from the plasma and hence suitable for our purpose. Unfortunately, the intensity of the peak is rather small because it arises from a multipole excitation of the electrons. In units of the strength of the surface (Fuchs-Kliwer) phonon at the vacuum-CaO interface, located at 524 cm⁻¹, which we take as a reference strength, the peak height was only around 10⁻⁶ for a 10 nm Al₂O₃ film with a plasma-induced surface charge density $n_s^p = 5 \cdot 10^{11} \text{ cm}^{-2}$ on top of a 30 nm CaO layer. Such a faint signal is most probably undetectable by current EELS instrumentation. In a recent application to nanoplasmonics⁴², for instance, EELS had a sensitivity of 10⁻⁴ in units of the elastic peak. Since the Fuchs-Kliwer phonon we use for normalization is typically an order of magnitude weaker than the elastic peak, signals should not be weaker than 10⁻³ in our units to be detectable.

Although electron counting techniques may advance⁴³, pushing thereby the sensitivity limit, we take 10⁻³ as a critical value. Measures are thus necessary to increase the signal strength up to this value. Increasing the signal strength by reducing the thickness of the substrate is not viable because it would threaten the mechanical stability. Another possibility is to increase the density of the electron gas by pre-n-doping the Al₂O₃ film. Due to the pre-doping a loss peak of lower order (and hence more intensity) becomes charge sensitive and hence suitable for charge diagnostics. It defines also a reference peak, present without surplus electrons from the plasma, which should help calibrating the method. The data presented below are therefore for a doped Al₂O₃ film. Due

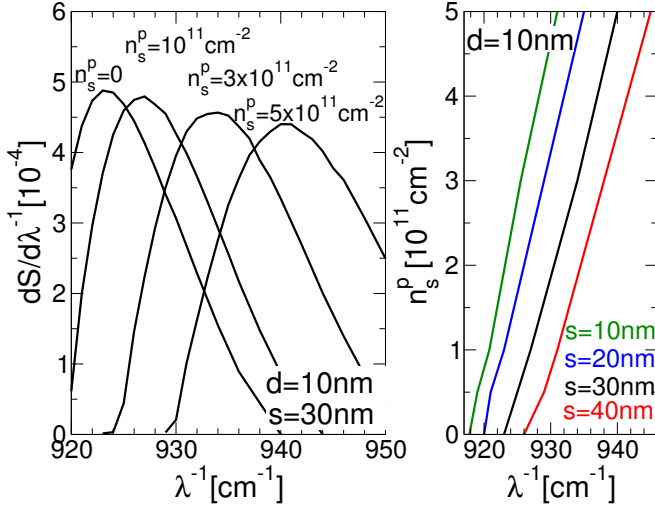


Figure 4: EELS spectra for an Al₂O₃/CaO structure at 300 K in the energy range where the resonance is located we use as a diagnostics for the plasma-induced charges in the Al₂O₃ film. The film's thickness and background doping are, respectively, $d = 10$ nm and $n_b^d = 10^{18}$ cm⁻³ corresponding to a surface charge density $n_s^d = n_b^d d = 10^{12}$ cm⁻². Left panel: Loss peak normalized to the strength of the Fuchs-Kliwer phonon of the vacuum-CaO interface as a function of the plasma-induced surface charge density n_s^p [corresponding to a bulk density $n_b^p = n_s^p/d$] for a substrate with thickness $s = 30$ nm. Right panel: Energetic position of the loss peak as a function of n_s^p for four different substrate thicknesses. The film thickness is in all four cases fixed to $d = 10$ nm.

to the doping the confinement potential is of course no longer simply the potential well arising from the electron affinities. The potential is affected by the Coulomb interaction between the electrons and should be calculated selfconsistently³⁵. But for demonstrating the basic principle of the charge measurement this is not necessary. We leave it thus for the future.

After these remarks let us now turn to the EELS spectrum of a stack with a pre-n-doped plasma-facing Al₂O₃ film. Figure 4 shows data for wave numbers where the loss is due to a fluctuation of the electron gas in a 10 nm film doped with a bulk electron density $n_b^d = 10^{18}$ cm⁻³. In the left panel the loss peak is plotted as a function of the density n_s^p of additional electrons coming from the plasma. Clearly, for a substrate thickness $s = 30$ nm the peak has not quite the required strength but reducing the substrate thickness a bit will push the strength above the critical value as will be discussed in the next paragraph. How the peak shifts with n_s^p for different substrate thicknesses is plotted in the right panel. Notice, the position of the peak for $n_s^p = 0$ depends weakly on s despite the unchanged bulk electron density in the film. We attribute this to a small substrate-induced redistribution of spectral weight due to changes in the electric field producing slightly different loss maxima. For all the chosen values of s the peak shifts nicely with n_s^p and is thus well suited for measuring n_s^p by simply recording

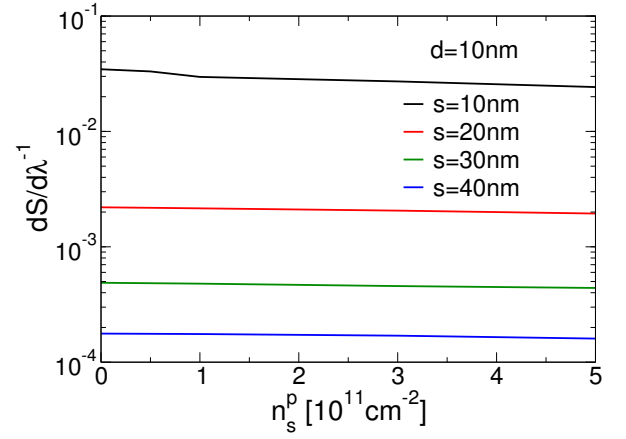


Figure 5: Intensity of the loss peaks shown in Fig. 4 as a function of n_s^p . The thicker the substrate the weaker the loss peak, as expected. The EELS spectrum is normalized to the intensity of the Fuchs-Kliwer phonon at the vacuum-CaO interface. As explained in the main text, we expect the critical strength below which the signal becomes undetectable to be around 10⁻³ in these units. Hence, the sensitivity of current EELS instrumentation may be not sufficient for substrates thicker than 30 nm.

the spectral position. Due to the limited energy resolution of EELS²⁴, experimentally detectable are only shifts larger than $\Delta\lambda^{-1} = 4$ cm⁻¹. Hence, charge densities $n_s^p > 10^{11}$ cm⁻² may be measurable by this technique. But this is also the range expected for plasma-facing dielectrics as can be inferred from experimental studies of the charging of dust particles in low-temperature plasmas⁴⁴ and measurements of the wall charge by the Pockels effect¹⁶⁻¹⁸.

The strength of the loss peaks is shown in Fig. 5. According to the considerations presented above we take 10⁻³ as the critical strength in units of the strength of the Fuchs-Kliwer phonon below which the signal cannot be detected anymore. As can be seen, the background doping pushes the signal strength for $s < 30$ nm above this critical value, leaving the system with $s = 30$ nm at the margin. Let us at this point however caution a bit. In the literature EELS data are mostly given in arbitrary units. Our estimate of the critical signal strength is based on one⁴² of the few publications where the data are normalized to a particular peak and hence estimable from an intensity point of view. It may be possible that electron detectors used in EELS are in fact more sensitive than we believe. The signal could then be accordingly weaker.

In order to understand the physics of the loss peak we are tracking as a function of n_s^p , we analyzed the spatial structure of the charge fluctuation giving rise to it using the procedure developed by Streight and Mills³³. They noticed that for ω residing on the loss peak and $q_{||}$ fixed to a value contributing to the EELS spectrum according to the ellipse equation (4) the z -dependence of the function $\text{Im}X(q_{||}, \omega, z)$, with $X(q_{||}, \omega, z)$ defined in (29), reflects the spatial form of the charge fluctuation asso-

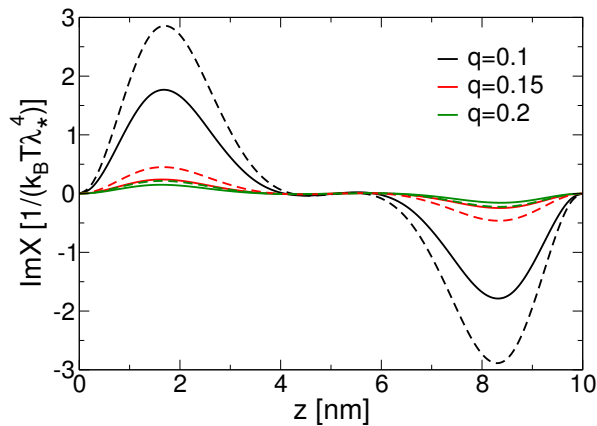


Figure 6: The function $\text{Im}X(q_{\parallel}, \omega, z)$ for an $\text{Al}_2\text{O}_3/\text{CaO}$ setup with $d = 10$ nm, $s = 30$ nm, $n_b^d = 10^{18} \text{ cm}^{-3}$ [corresponding to $n_s^d = 10^{12} \text{ cm}^{-2}$], and two values for the density of the plasma-induced surplus electrons: $n_s^p = 10^{11} \text{ cm}^{-2}$ (solid lines) and $n_s^p = 5 \cdot 10^{11} \text{ cm}^{-2}$ (dashed lines). The lateral momentum q_{\parallel} in units of $(\lambda_*)^{-1} = 1/\sqrt{\hbar^2/2m_e^*k_B T}$ and the energy $\hbar\omega$ in units of wave numbers making in each case $P(q_{\parallel}, \omega)$ maximal are given by $(0.1, 927.742 \text{ cm}^{-1})$, $(0.15, 923.538 \text{ cm}^{-1})$, and $(0.2, 921.318 \text{ cm}^{-1})$ for $n_s^p = 10^{11} \text{ cm}^{-2}$ and $(0.1, 941.837 \text{ cm}^{-1})$, $(0.15, 936.1 \text{ cm}^{-1})$, and $(0.2, 932.691 \text{ cm}^{-1})$ for $n_s^p = 5 \cdot 10^{11} \text{ cm}^{-2}$. For each density the three doubles belong to the domain D over which $P(q_{\parallel}, \omega)$ has to be integrated according to (1). The z -dependence of $\text{Im}X(q_{\parallel}, \omega, z)$ shows that the charge fluctuation giving rise to the peak in $P(q_{\parallel}, \omega)$ is a surface plasmon localized close to the boundaries of the Al_2O_3 film.

ciated with the peak. Figure 6 shows this function for two different values of n_s^p for a structure with $d = 10$ nm, $s = 30$ nm, and $n_b^d = 10^{18} \text{ cm}^{-3}$. The three doubles $(q_{\parallel}, \hbar\omega)$ are in each case fixed to the value where $P(q_{\parallel}, \omega)$ is maximal. Since the potential well confining the electrons to the film is in our crude model infinitely deep the charge fluctuations are in all cases symmetric with respect to the film center. The fluctuation is maximal close to the boundaries of the film. Hence, it represents a surface plasmon. Increasing the density n_s^p changes mainly the amplitude of the oscillation. The overall structure remains the same. Hence, we are indeed tracking a particular surface plasmon of the film with the density of the surplus electrons coming from the plasma.

At the end of this section let us demonstrate the need for using the nonlocal response theory of Mills and coworkers^{31–33}. It is necessary in cases where the screening length $\lambda_s = \sqrt{k_B T / 4\pi n_b e^2}$ due to the electrons producing the charge fluctuation the EELS electron couples to is on the same order as the (thermal) de Broglie wave length $\lambda_{dB} = \sqrt{(2\pi\hbar)^2 / 3m_e^* k_B T}$. The density $n_b = n_b^d + n_b^p$ with n_b^d the bulk electron density due to the background doping and n_b^p the bulk density of the electrons coming from the plasma (corresponding to a surface density $n_s^p = n_b^p d$). As can be seen in Table II, the screening length and de Broglie wavelength, given for

d/nm	Al_2O_3 ($\lambda_{dB} = 9.9$ nm)		
	$n_s^p [10^{11} \text{ cm}^{-2}]$	$n_b [10^{18} \text{ cm}^{-3}]$	$\lambda_s [\text{nm}]$
5	1	1.2	3.3
10	1	1.1	3.4
15	1	1.07	3.5

Table II: Comparison of the de Broglie wave length λ_{dB} and screening length λ_s for an Al_2O_3 film with thickness d and charge density $n_b = n_b^d + n_b^p$, where n_b^d is the film's background electron density due to doping, to be taken in all cases as 10^{18} cm^{-3} , and $n_b^p = n_s^p/d$ the density of the additional electrons coming from the plasma. As can be seen λ_{dB} and λ_s are on the same order. Hence, a nonlocal description of the modification of the film's dielectric function due to the charge carriers is required.

three different values of d and an electron density typical for our setup, are on the same order. The nonlocal theory is thus required to describe the dielectric response of the electrons in the film. In fact, the loss peak we are monitoring is even absent in the local theory which uses a simple Drude term added to the film's background dielectric function²⁰.

IV. CONCLUSIONS

We described an EELS setup for determining the density of electrons accumulated by a plasma-facing dielectric solid. It is based on a two-layer structure, consisting of a film and a substrate, which can be inserted into the wall of a discharge. The film is made out of the material whose plasma-induced charging one wants to know while the substrate ensures the stability of the structure and the confinement of the charges to the film. It is also the layer to which the probing electron beam is applied. The device is geared towards measuring the total charge accumulated by the plasma-facing structure. In principle a structure of this type could be also used to determine by EELS the profile of the charge distribution perpendicular to the plasma-solid interface. It is then however necessary to base the theoretical analysis on a selfconsistent kinetic theory of the electric double layer at the plasma-solid interface because otherwise the width of the space charge cannot be determined. In addition the film has to host the whole space charge. How challenging this will be for the EELS sensitivity limit future work will show.

The main goal of this work was to find an EELS setup for measuring the total charge residing inside a plasma-facing dielectric film. For that purpose we made simplifying assumptions and neglected a number of aspects which may be of importance for a quantitative analysis of experimental data. For instance, the plasma in front of the structure is not modelled, it simply provides surplus charges/electrons for the film. Furthermore, the charge confinement is not calculated selfconsistently and the charges inside film are assumed to be thermalized.

It is also assumed that all the electrons coming from the plasma are accumulated in the film's conduction band ignoring surface states. These factors will modify the EELS spectrum quantitatively but not qualitatively. The principle of our proposal—confining the wall charge to a narrow film, stabilizing the film by a substrate, and reading-out the charge density from the shift of a loss peak in the from-the-back EELS—is unaffected by them.

To obtain in the particular scattering geometry on which our proposal is based a sufficiently strong loss peak, detectable by current EELS instrumentation, it is most probably necessary to pre-n-dope the plasma-facing film. For the principle of the method the doping is not necessary. The undoped film has loss peaks due exclusively to plasma-induced charging but they are rather faint because of their multipole character. The pre-doping has however also the nice additional effect of providing a reference peak, present also when the plasma is off. Once the plasma is on and the film is flooded

by electrons from the plasma the peak shifts with the density of the additional electrons. From the peak position the density can thus be determined. Our results for the $\text{Al}_2\text{O}_3/\text{CaO}$ system indicate that the from-the-back geometry may indeed work. By a judicious choice of materials—having suitable mechanical properties, conduction band edges with appropriate off-sets, and a suite of donors—it should be possible to build sub-100 nm thick structures for measuring the wall charge which are mechanically stable and yet furnish the EELS signal with enough strength to be detectable.

Acknowledgments

In the initial stages this work was supported by the Deutsche Forschungsgemeinschaft through the Transregional Collaborative Research Center SFB/TRR24.

-
- ¹ F. X. Bronold and H. Fehske, J. Phys. D: Appl. Phys. **50**, 294003 (2017).
 - ² M. A. Lieberman and A. J. Lichtenberg, *Principles of Plasma Discharges and Materials Processing* (Wiley-Interscience, New York, 2005).
 - ³ I. Langmuir and H. Mott-Smith, Gen. Electr. Rev. **27**, 449 (1924).
 - ⁴ J. G. Eden, S. J. Park, J. H. Cho, M. H. Kim, T. J. Houlihan, B. Li, E. S. Kim, T. L. Kim, S. K. Lee, K. S. Kim, et al., IEEE Trans. Plasma Sci. **41**, 661 (2013).
 - ⁵ K.-F. Chen and J. G. Eden, Appl. Phys. Lett. **93**, 161501 (2008).
 - ⁶ M. Tabib-Azar and P. Pai, Micromachines **8**, 117 (2017).
 - ⁷ C. J. Wagner, P. A. Tschertchian, and J. G. Eden, Appl. Phys. Lett. **97**, 134102 (2010).
 - ⁸ E. Kindel and R. Arndt, Beitr. Plasmaphysik **20**, 119 (1980).
 - ⁹ M. Li, C. Li, H. Zhan, J. Xu, and X. Wang, Appl. Phys. Lett. **92**, 031503 (2008).
 - ¹⁰ D. F. Opaitis, M. N. Shneider, R. B. Miles, A. V. Likhanskii, and S. O. Macheret, Phys. Plasmas **15**, 073505 (2008).
 - ¹¹ I. Radu, R. Bartnikas, and M. R. Wertheimer, J. Phys. D: Appl. Phys. **36**, 1284 (2003).
 - ¹² K. Pangal, S. L. Firebaugh, and J. C. Sturm, Appl. Phys. Lett. **69**, 1471 (1996).
 - ¹³ P. Viegas, E. Slikboer, A. Obrušnik, Z. Bonaventura, A. Sobota, E. Garcia-Caurel, O. Guaitella, and A. Bourdon, Plasma Sources Sci. Technol. **27**, 094002 (2018).
 - ¹⁴ R. Tschiersch, M. Bogaczyk, and H.-E. Wagner, J. Phys. D: Appl. Phys. **47**, 365204 (2014).
 - ¹⁵ M. Bogaczyk, R. Wild, L. Stollenwerk, and H.-E. Wagner, J. Phys. D: Appl. Phys. **45**, 465202 (2012).
 - ¹⁶ F. Gégot, T. Callegari, M. Aillerie, and J. P. Boeuf, J. Phys. D: Appl. Phys. **41**, 135204 (2008).
 - ¹⁷ T. Sakurai, H. Yoda, T. Terayama, K. Ishii, and Y. Murakami, Japan. J. Appl. Phys. **46**, 3596 (2007).
 - ¹⁸ D. C. Jeong, H. S. Bae, and K. W. Whang, J. Appl. Phys. **97**, 013304 (2005).
 - ¹⁹ K. Rasek, F. X. Bronold, and H. Fehske, Europhys. Lett. **124**, 25001 (2018).
 - ²⁰ H. Ibach and D. L. Mills, *Electron Energy Loss Spectroscopy and Surface Vibrations* (Academic Press, New York, 1982).
 - ²¹ P. Lambin, J. P. Vigneron, and A. A. Lucas, Phys. Rev. B **32**, 8203 (1985).
 - ²² P. A. Thiry, M. Liehr, J. J. Pireaux, and R. Caudano, Phys. Scripta **35**, 368 (1987).
 - ²³ H. Ibach, Surf. Sci. **299/300**, 116 (1994).
 - ²⁴ A. Rizzi, Fresenius J. Anal. Chem. **358**, 15 (1997).
 - ²⁵ H. Lüth, *Solid Surfaces, Interfaces and Thin Films* (Springer-Verlag, Berlin, Heidelberg, 2015).
 - ²⁶ H. Lüth, Vacuum **38**, 223 (1988).
 - ²⁷ H. Lüth, Surf. Sci. **168**, 773 (1986).
 - ²⁸ A. Ritz and H. Lüth, Phys. Rev. Lett. **52**, 1242 (1984).
 - ²⁹ H. Lüth, Surf. Sci. **126**, 126 (1983).
 - ³⁰ I. Mahboob, T. D. Veal, C. F. McConville, H. Lu, and W. J. Schaff, Phys. Rev. Lett. **92**, 036804 (2004).
 - ³¹ D. Mills, Surf. Sci. **48**, 59 (1975).
 - ³² D. H. Ehlers and D. L. Mills, Phys. Rev. B **36**, 1051 (1987).
 - ³³ S. R. Streight and D. L. Mills, Phys. Rev. B **40**, 10488 (1989).
 - ³⁴ S. Gasiorowicz, *Quantum Physics* (John Wiley & Sons, New York, 1974).
 - ³⁵ S. R. Streight and D. L. Mills, Phys. Rev. B **37**, 965 (1988).
 - ³⁶ A. M. Hofmeister, E. Keppel, and A. K. Speck, Mon. Not. R. Astron. Soc. **345**, 16 (2003).
 - ³⁷ E. D. Palik, *Handbook of Optical Constants of Solids* (Academic, 1985).
 - ³⁸ A. S. Barker, Phys. Reports **132**, 1474 (1963).
 - ³⁹ M. L. Huang, Y. C. Chang, C. H. Chang, T. D. Lin, J. Kwo, T. B. Wu, and M. Hong, Appl. Phys. Lett. **89**, 012903 (2006).
 - ⁴⁰ A. M. Stoneham and M. J. L. Sangster, Phil. Mag. B **43**, 609 (1981).
 - ⁴¹ A. Tselev, J. Velmurugan, A. V. Ievlev, and S. V. Kalinin, ACS Nano **10**, 3562 (2016).
 - ⁴² M. Bosman, E. Ye, S. F. Tan, C. A. Nijhuis, J. K. W. Yang, R. Marty, A. Mlayah, A. Arbouet, C. Girard, and

- M.-Y. Han, Sci. Reports **3**, 1312 (2013).
- ⁴³ J. L. Hart, A. C. Lang, A. C. Leff, P. Longo, C. Trevor, R. D. Twisten, and M. L. Taheri, Sci. Reports **7**, 8243 (2017).
- ⁴⁴ S. A. Khrapak, S. V. Ratynskaia, A. V. Zobnin, A. D. Usachev, V. V. Yaroshenko, M. H. Thoma, M. Kretschmer, H. Hoefner, G. E. Morfill, O. F. Petrov, et al., Phys. Rev. E **72**, 016406 (2005).